Aerobic exercise promotes PDAC vascular normalization through S1PR1 signaling in tumor endothelial cells

[a]Riccardo Ballarò, [a]Sumedha Pareek, [a]Jonghae Lee, [a]Hetal Patel, [a]Priya Tirumala, [a]Guanshu Liu, [a]Karma Hayek, [a]Hannah Savage, [a]Bella Guerrouahen, [b]An Ngo-Huang, [c]Nathan Parker, [d]Matthew HG Katz, [e]Maria Petzel, [f]Florencia McAllister, [d,f]Robin Wright, [g]Lin Tan, [g]Philip L Lorenzi and [a]Keri Schadler.*

[a]Department of Pediatrics Research, The University of Texas MD Anderson Cancer Center, MD Anderson Cancer Center, Texas, USA.

[b]Department of Palliative, Rehabilitation, and Integrative Medicine, The University of Texas MD Anderson Cancer Center, Houston, Texas, USA.

[c]Department of Health Outcomes and Behavior, Moffitt Cancer Center, Tampa, Florida, USA.

[d]Department of Surgical Oncology, The University of Texas MD Anderson Cancer Center, Houston, Texas, USA.

[e]Department of Clinical Nutrition, The University of Texas MD Anderson Cancer Center, Houston, Texas, USA.

[f]Department of Clinical Cancer Prevention, The University of Texas MD Anderson Cancer Center, Houston, Texas, USA.

[g]Department of Bioinformatics and Computational Biology, The University of Texas MD Anderson Cancer Center, Houston, Texas, USA.

Abstract

Pancreatic Ductal Adenocarcinoma (PDAC) is characterized by high resistance to anti-cancer therapies. This resistance is caused in part by hypo-vascularization and dysfunctional vessels which inefficiently deliver chemotherapy. Here, we define the mechanism of aerobic exercise-induced tumor vascular remodeling and improved chemotherapy delivery and efficacy. We found that aerobic exercise was able to improve tumor vascular function and increase the number of lymphatic vessels, and these effects were associated with increased gemcitabine delivery to and efficacy against PDAC in mice. Further, exercise increased sphingosine-1-phosphate (S1P) in plasma and the activation of sphingosine-1-phosphate receptor 1 (S1PR1) in tumor endothelial cells. S1PR1 endothelial cell-specific deletion blunted the exercise-induced improvements in tumor vascular function, gemcitabine efficacy and drug concentration. Preclinical findings were validated in a patient cohort in which we found that exercise during neoadjuvant chemotherapy remodeled PDAC vasculature and improved tumor vascular function. These findings provide direct evidence that exercise increases chemotherapy delivery and efficacy by improving vascular function, defining S1PR1 as a necessary mediator of exercise-induced vascular remodeling.

***** Corresponding author

Introduction

Pancreatic Ductal Adenocarcinoma (PDAC) is the third leading cause of cancer-related death in the Unites States, with an overall 5-year survival of 12%[1]. Although the recent treatment advances for PDAC have improved the outcome of resectable localized tumors, approximately 80% of patients with PDAC are not candidates for curative surgery[2]. Various combinations of systemic chemotherapy with or without radiation have been used over the past several decades with little progress toward better outcomes[3]. These poor results reflect the aggressive biology of PDAC cells, along with the complex tumor microenvironment which promotes cancer proliferation, metastasis and therapeutic resistance[4]. The PDAC microenvironment is composed of poorly formed and dysfunctional vessels, cancer-associated fibroblasts, dense extracellular matrix, and largely suppressive immune cell populations[5]. Although dysfunctional vasculature is a common feature of most solid tumors, PDAC vasculature is particularly insufficient for drug delivery to the tumor because most PDAC tumors have low abundance of blood vessels in addition to the dysfunction of existing vessels[6]. The vascular dysfunction is compounded by the dense stroma, which increases intratumoral solid stress, causing vessel collapse[7]. These vascular alterations, together with insufficient lymphatic drainage, result in high interstitial fluid pressure, ultimately preventing drugs from accessing the tumor[8–10]. Promoting the formation of functional vessels may be an effective strategy to increase chemotherapy efficacy and decrease cancer dissemination.

We previously demonstrated that aerobic exercise positively impacts tumor vasculature in mice[11–14]. Exercise remodeled melanoma vasculature, increasing microvessel density, the number of long vessels and vessels with open lumens[11,15]. Similarly, aerobic exercise improved Ewing sarcoma-bearing mouse vasculature and chemotherapy efficacy and these effects were associated with increased S1PR1 expression in tumor endothelial cells[14]. The exercise-induced remodeling of tumor vasculature was also observed in a subcutaneous PDAC patient-derived xenograft and syngeneic PDAC cell line in mice[11,12]. However, the subcutaneous location of these tumor models is unlikely to reflect the correct tumor microenvironment, making them inferior models for defining the relationship between exercise and PDAC tumor vasculature. Here, we evaluate the effects of aerobic exercise on orthotopic PDAC vasculature and response to therapy. Further, we utilize an orthotopic PDAC model to define the molecular regulation of the tumor vascular response to exercise.

Vascular maturation and function are regulated by a family of G-coupled receptors, the S1P receptors (S1PRs), which are activated by the ligand sphingosine-1 phosphate (S1P)[16]. S1PR1, S1PR2 and S1PR3 are expressed by endothelial cells and together regulate vascular development, tone and permeability[16]. S1PR1 signaling in response to S1P suppresses VEGF-dependent vascular sprouting, induces adherens junction assembly, and enhances integrin activation as a fundamental mechanism for vascular stabilization and efficient perfusion[17]. In addition, S1PR1 regulates the interaction of perivascular and endothelial cells in the microvasculature to generate mature, functional vessels[18]. Deletion of the *s1pr1* gene is embryonically lethal due to defective neovascularization[19,20]. Post-natal endothelial cell-specific deletion of *s1pr1* impairs vascular architecture, permeability and barrier function[21]. S1PR1 has also been shown to be an important regulator of tumor vessel function[22,23].

We demonstrate that exercise improves tumor blood and lymphatic vessels, and that the remodeling of PDAC vasculature by exercise is associated with increased plasma S1P and S1PR1 activation in tumor vascular endothelial cells. Exercise also reduced peritoneal spreading of PDAC. Our findings show that S1PR1 expression is necessary for the tumor vascular improvements and for the increased

81 chemotherapy delivery and efficacy induced by exercise in PDAC-bearing mice, establishing a causal
82 effect between improved tumor vasculature and increased chemotherapy response in tumors upon
83 exercise. Further, we validate the relationship between exercise and vasculature in a human PDAC
84 dataset, showing that increased physical activity in PDAC patients remodels tumor vasculature and
85 reduces tumor vascular leakage.

86 **Methods**

87 **Cell culture**

88 PDAC KPC-4662 cells were derived from *Kras*$^{LSL-G12D/+}$; *Trp53*$^{LSL-R172H/+}$; *Pdx1-Cre* mice and provided by Dr.
89 Robert Vonderheide (University of Pennsylvania School of Medicine). Hy 15549 cells were derived from
90 *Kras*$^{LSL-G12D/+}$; Trp53$^{lox/+}$; *Ptf1a-Cre* mice and provided by Dr. Haoqiang Ying (The University of Texas MD
91 Anderson Cancer Center). Cells were cultured in DMEM (Gibco 11965092; KPC-4662) or RPMI (Corning
92 10-040-CV; Hy15549) containing 10% FBS (Sigma-Aldrich, F2442), 100 U/mL penicillin, and 100 mg/mL
93 streptomycin (Gibco, 15140122). Cells were passaged by dissociation with Accutase (Sigma-Aldrich,
94 A6964) and maintained at 37°C, 95% relative humidity, and 5% CO_2. Cells were routinely confirmed as
95 Mycoplasma negative by qRT-PCR with primers forward 5'-GGGAGCAAACAGGATTAGATACCCT-3' and
96 reverse 5'- TGCACCATCTGTCACTCTGTTAACCTC-3', or by analysis with MycoAlert Mycolplasma Detection
97 Kit (Lonza, LT07-418).

98 **Mouse strains**

99 The Institutional Animal Care and Use Committee at The University of Texas MD Anderson Cancer
100 Center approved all animal studies. Mice were housed in cohorts of three to five animals per cage, in
101 individually ventilated cages under pathogen-free conditions. Animals had free access to food and water
102 and were kept on a 12-hour light/12-hour dark cycle. C57BL/6J wild-type mice were purchased from The
103 MD Anderson Experimental Radiation Oncology Mouse Facility or Jackson Laboratory. S1PR1 GFP
104 signaling reporter mice were previously described[24]. Briefly, B6N.129S6(FVB)-*S1pr1*$^{tm3.1(tTA,-Arrb2)Rlp/J}$ mice
105 (Jackson Laboratory, stock #026275) were crossed with pTRE-H2BGFP mice (Jackson Laboratory, stock
106 #005104) for the generation of a mouse carrying a S1PR1 knock-in with tetracycline-regulated
107 transactivator (tTA)-tobacco etch virus (TEV) protease recognition sequence (tevs) fusion protein and an
108 *Arrb2* (murine β-arrestin)-TEV protease fusion protein, and the transgene expressing the human histone
109 1 (H2BJ) protein and Green Fluorescent Protein (GFP) fusion protein under the control of a tetracycline-
110 responsive promoter element (TRE; tetO). pTRE-H2BGFP were purchased with a BALB/c background and
111 were backcrossed 7 times with C57BL/6J mice before being used for experiments. Mice expressing one
112 allele of both transgenes were considered S1PR1 GFP reporter mice. Littermates expressing only the
113 H2BJ-GFP allele without the S1PR1 knock-in were used as controls[24]. Endothelial cell-specific *S1pr1*
114 knockout mice (*S1pr1*$^{LoxP/LoxP}$ *Cdh5-Cre*-ER^{T2}; S1PR1 EKO) were previously described[20]. Briefly, mice
115 carrying *loxP* sites flanking *S1pr1* gene (*S1pr1*$^{loxP/loxP}$; S1PR1 WT; Jackson Laboratory, stock # 019141)
116 were crossed with mice expressing Cre recombinase (*Cre*-ER^{T2}) under the vascular endothelial cadherin
117 (*Cdh5*) promoter (*Cdh5-Cre*ER^{T2}; Taconic # 13073). Gene deletion by the Cre recombinase was achieved
118 with tamoxifen (Sigma-Aldrich, T5648; 100 mg/kg per day) treatment by oral gavage at 6-9 weeks of age
119 for five consecutive days, and mice were allowed to recover for 12 days before being used for
120 experiments. Mouse genotyping was performed using ear punches. The genotype and phenotype of
121 these mice was verified by analyzing the DNA recombination in lungs and by immunofluorescence in
122 tumor tissue, respectively (**Supplementary Fig. 1a, b**).

123 **Tumor cell injection, experimental protocol and exercise regimen in mice**

124 KPC-4662 (1.25 x 10^5 suspended in cell medium) or Hy 15546 cells (1 x 10^4 suspended in Hank's Buffered
125 Saline Solution) were injected into the mouse pancreas in 20µl volume, during aseptic surgery. Briefly,
126 an incision was made in the left flank and tumor cells were injected using a 30-gauge needle into the tail
127 of the pancreas. The peritoneum was sutured with 4-0 Vicryl and the skin was closed with wound clips.
128 To calculate the tumor volume, two tangential ultrasound images along the longitudinal and transverse
129 planes were used. Tumor volume was calculated by the formula 4/3 π ABC, where A, B and C are the
130 measured diameters of each tumor using NIH open-source image software ImageJ (http://rsbweb.nih.
131 gov/ij/; **Supplementary Figure 1c**). Tumor volumes were then measured once per week by the same
132 method.

133 *Experimental protocol 1: exercise 8 and 16 meters per minute (m/min)*

134 At day 8 after KPC-4662 or Hy 15549 injection, tumor volume was measured by ultrasound using Vevo
135 3100 with a 40-MHz linear signal transducer and 550D probe (Fujifilm, VisualSonics), and mice were
136 divided by tumor size to the different experimental groups: sedentary (Sed; n= 9 KCP-4662; n=10 Hy
137 15549), exercise 8 m/min (Ex 8; n=9 KPC-4662; n=10 Hy 15549) and exercise 16 m/min (Ex 16; n=9 KPC-
138 4662; n=10 Hy 15549). Vascular function (vessel perfusion and leakage) and hypoxia in KPC-4662 mice
139 were assessed in different experiments using the same conditions except for the experimental groups,
140 which included only Sed (n=11-10) and Ex 16 (n=10). Mice underwent the acclimatization protocol on
141 treadmills (Exer 3/6 Treadmill; Columbus Instruments) at day 9 and 10 after tumor injection. For the 8
142 m/min exercise protocol, acclimatization consisted of exercise at 3 m/min for 20 minutes on day 9, and
143 at 6 m/min for 40 minutes on day 10 (**Supplementary Figure 1d**). For the 16 m/min exercise protocol, on
144 day 9 mice ran at 8 m/min for 20 minutes and on day 10 at 12 m/min for 40 minutes. Mice started the
145 full exercise regimen after tumors reached ~ 30 mm^2 (day 12; 8 m/min or 16 m/min for 45 minutes, 5
146 days a week for around 3 weeks; **Supplementary Figure 1d**). All mice were humanely euthanized at day
147 29-31 by cervical dislocation under isoflurane anesthesia 48 hours after the final exercise session.

148 *Experimental protocol 2: exercise 16 m/min in S1PR1 GFP reporter mice*

149 KPC-4662 cells were injected as described above into S1PR1 GFP reporter mice (B6N.129S6(FVB)-
150 *S1pr1*$^{tm3.1(tTA,-Arrb2)Rlp/J}$ x pTRE-H2BGFP mice). At day 8 after KPC-4662 cell injection, were divided into two
151 groups: Sed (n=7) or Ex (exercise 16 m/min; n=7). Mice underwent the acclimatization protocol and full
152 exercise regimen as described above. pTRE-H2BGFP mice (n=2) were also added to the experiment as a
153 negative control for GFP fluorescence. Only mice that survived until the end of the experimental
154 protocol were used for flow cytometry analysis of S1PR1 activation (Sed, n=6; Ex, n=5). All mice were
155 humanely euthanized as described above.

156 *Experimental protocol 3: exercise 16 m/min + gemcitabine in S1PR1 WT mice*

157 At day 8 after KPC-4662 cell injection, *S1pr1*$^{loxP/loxP}$ (S1PR1 WT) mice were randomized in Sed (n=11), Ex
158 (exercise 16 m/min; n=11), Gem (gemcitabine; n=11) and Ex+Gem (exercise+gemcitabine; n=11). Mice
159 underwent the acclimatization protocol and full exercise regimen as described above. Mice were treated
160 with intravenous (i.v.) injections of 25 mg/kg gemcitabine (Sagent Pharmaceuticals, 25021-235-50) after
161 the exercise session, twice per week, for 3 weeks). All mice were humanely euthanized as described
162 above.

163 *Experimental protocol 4: exercise 16 m/min + gemcitabine in S1PR1 WT and S1PR1 EKO mice*

164 Both S1PR1 WT (*S1pr1*$^{loxP/loxP}$) and S1PR1 EKO (*S1pr1*$^{LoxP/LoxP}$ *Cdh5-Cre*-ER^{T2}) mice were treated with
165 tamoxifen as described above. At day 8 after KPC-4662 cell injection, S1PR1 EKO mice were randomized
166 in Sed (n=10), Ex (exercise 16 m/min; n=10), Gem (gemcitabine; n=11) and Ex+Gem
167 (exercise+gemcitabine; n=11). S1PR1 WT mice (n=11) were also added to the experiment as a control
168 and for the evaluation of basal differences between S1PR1 and EKO groups. Mice underwent the
169 acclimatization protocol, full exercise regimen, chemotherapy treatment and terminal euthanasia as
170 described above.

171 **Peritoneal carcinomatosis (PCI) analysis**

172 The PCI analysis was performed using a scoring system adapted from Bastiaenen *et al.*[25]. At the time of
173 necropsy, mice were evaluated for the presence of macroscopic metastases in different areas and
174 organs of the peritoneum (liver, diaphragm, spleen, intestine, peritoneum wall). Per organ or region, a
175 score of 0-3 was determined based on the number and size of nodules. No macroscopic metastasis was
176 scored as 0; tumor ≤ 2mm was scored as 1; tumors 2-5mm or 2 - 5 tumors was scored as 2; tumor ≥
177 5mm or > 10 tumors was scored as 3. The PCI of each animal was calculated by adding scores of all the
178 different regions within the animal together.

179 **Immunofluorescence Staining**

180 For frozen sections of mouse tumors, tissues were fixed in 4% PFA for 1 hour at 4°C. Tissues were
181 washed three times in PBS, incubated for 48 hours with rocking at 4°C in 30% sucrose and embedded in
182 OCT compound. Frozen sections were cut at 10 µm thickness. Tissue sections were fixed with cold
183 acetone for 8 minutes at -20°C, then washed three times in PBS before blocking with 4% fish gel blocking
184 solution (CWFS 900.0033, Aurion) in PBS for 1 hour at room temperature. Primary antibodies were
185 diluted in blocking solution and incubated at 4°C overnight. Slides were washed three times with PBS
186 after the overnight incubation. Secondary conjugated antibodies were diluted in blocking solution and
187 incubated for 1 hour at room temperature. Slides were mounted with Fluoro-Gel II with DAPI solution to
188 stain the nuclei (Electron Microscopy Science, 17985-50). The following antibodies and dilutions were
189 used: rat anti-mouse CD31 1:50 (BD Biosciences, 550274), goat anti-mouse CD31 1:50 (R&D Systems,
190 AF3628), rat anti-mouse LYVE-1 1:50 (Santa Cruz Biotechnology, sc-65647), rabbit anti-mouse Albumin
191 1:100 (Proteintech, 16475-1-AP), rabbit anti-mouse/human αSMA 1:100 (Abcam, ab5694), rabbit anti-
192 mouse NG2 1:200 (EMD Millipore, AB5320), rabbit anti-mouse Desmin 1:200 (Abcam, ab15200), rat anti-
193 mouse S1PR1 1:50 (R&D Systems, MAB7089). The following secondary antibodies and dilutions were
194 used: goat anti-rat Alexa Fluor 488 1:1000 (Thermo Fisher Scientific, A-11006), goat anti-rat Alexa Fluor
195 594 1:1000 (Thermo Fisher Scientific, A-11007), donkey anti-rabbit Alexa Fluor 647 1:1000 (Thermo
196 Fisher Scientific, A-31573), goat anti-rabbit Texas Red 1:1000 (Thermo Fisher Scientific, T-2767), donkey
197 anti-goat 647 1:1000 (Thermo Fisher Scientific, A21447).

198 For human tissue, paraffin-embedded slides were deparaffinized using xylenes and ethanol. Antigen
199 retrieval was performed in 10mM Tris Base, 1mM EDTA solution for 20 minutes. Slides were washed
200 three times in PBS before blocking with 4% fish gel blocking solution (CWFS 900.0033, Aurion) in PBS for
201 30 minutes at room temperature. Primary antibodies were diluted in blocking solution and incubated at
202 4°C overnight. Slides were washed three times with PBS after the overnight incubation. The following
203 primary antibodies and dilutions were used: rabbit anti-human CD31 1:50 (Abcam, ab28364) and goat

204 anti-human Albumin 1:50 (Abcam, ab19194). Secondary conjugated antibodies were diluted in blocking
205 solution and incubated for 1 hour and 30 minutes each at room temperature. Secondary incubation for
206 the two different secondaries used was performed in two separate steps of 1 hour and 30 minutes each,
207 spaced out by three PBS washes. The following secondary antibodies and dilutions were used: donkey
208 anti-goat 647 1:500 (Thermo Fisher Scientific, A21447) and goat anti-rabbit 594 1:1000 (Thermo Fisher
209 Scientific, A-11012). Slides were mounted with Fluoro-Gel II with DAPI solution to stain the nuclei
210 (Electron Microscopy Science, 17985-50).

211 **Tumor hypoxia and vessel perfusion**

212 To evaluate the number of perfused vessels, mice were injected via tail vein with 100 µL Lycopersicon
213 esculentum (Tomato) Lectin-LEA DyLight (1 mg/mL; Invitrogen, L32471) and euthanized after ten
214 minutes. Tumors were excised and processed for immunofluorescent staining as described above. For
215 tumor hypoxia analysis, mice were injected via tail vein with 100µL Hypoxyprobe-1 (pimonidazole HCl;
216 18 mg/ml; Hypoxyprobe Inc., HP6-200Kit) and euthanized after one hour. Tumors were processed for
217 immunofluorescence staining and incubated with FITC conjugated to mouse IgG1 monoclonal antibody
218 (FITC-Mab1; Hypoxyprobe Inc, 1:75) diluted in 4% fish gel blocking solution overnight at 4C. Whole
219 tumor tile scan images were captured using Leica LAS X software. The hypoxia area of tumor sections
220 was calculated by normalizing hypoxyprobe-1$^+$ area to total number of nuclei. Area of total lectin$^+$ signal
221 was normalized by total CD31$^+$ area. Sample numerosity for these analyses may vary from the original
222 mouse number because for very ill mice, i.v. injection of the hypoxyprobe-1 or lectin was deemed to be
223 ineffective and therefore hypoxia and vessel perfusion were not analyzed in those mice.

224 **Tumor vascular image analysis**

225 Five to nine images were randomly captured at 10x magnification across each tumor and stained as
226 described above. Quantifications were performed on each image and all image quantifications
227 corresponding to a sample were averaged to report one value per tumor on graphs. Images were
228 captured using a Leica fluorescence microscope (DMi8; Leica Microsystems Inc.) with LAS X software.
229 Image analyses were performed using ImageJ. Tumor vessel structural analysis was performed as
230 described previously[11]. Vessel parameters included the total number of CD31$^+$ vessels, the percentage of
231 visible open lumens over total vessels, the percentage of vessels with a length >100 µm (elongated
232 vessels), and the number of 100 µm^2 regions per image occupied by CD31$^+$ vessels (microvessel density).
233 Specifically, the microvessel density was calculated by dividing the image area into equal squares (100
234 µm^2) creating a grid. The number of squares in the grid occupied by CD31$^+$ vessels was counted, and
235 total number of squares are reported as microvessel density. For evaluating the pericytes coverage of
236 blood vessels, the pericyte markers αSMA, desmin or NG2 were costained with CD31. Pericytes coverage
237 was quantified as the colocalization between pericyte markers and CD31 fluorescence area.

238 **Flow cytometry**

239 KPC-4662 tumors from sedentary and exercised mice were harvested and immediately digested in HBSS
240 with DNase I (100 µg/mL; Roche, 04716728001) and collagenase type II (10mg/ml; Worthington,
241 LS004176) for 45 minutes at 37°C. Reb blood cells were lysed using Ammonium-Chloride-Potassium
242 (ACK) lysing buffer (Thermofisher Scientific, A1049201) for 5 minutes on ice. Single-cell suspensions
243 were prepared using a 100 µm nylon mesh. Cells were blocked for 15 minutes at room temperature
244 using purified rat anti-mouse CD16/CD32 (BD Biosciences, 553141). Cells were stained with

245 fluorochrome-conjugated antibodies for 15 minutes at room temperature, followed by dead cell staining
246 with aqua fluorescent reactive dye (Invitrogen, 2456941) for 20 minutes and then fixed with stabilizing
247 fixative (BD Biosciences, 338036). Data were acquired using an LSR Fortessa flow cytometer (BD
248 Biosciences) and analyzed with FlowJo software version 10. Fluorochrome-conjugated antibodies used
249 for flow cytometry were CD45 Pacific Blue (Biolegend, 103126) and CD31 PE-Cy7 (Invitrogen, 25-0311-
250 82).

251 **Analysis of S1P by Triple Quadruple LC-MS**

252 Blood from sedentary or exercised mice was collected by retro orbital bleeding in EDTA collection tubes
253 2 hours after the last bout of exercise. Blood was centrifuged twice at 2000 g for 10 minutes to pellet
254 the cellular component and the supernatant was collected in a new tube after each centrifugation.
255 Analysis was performed by the Metabolomics Core Facility at MD Anderson Cancer Center. To
256 determine the relative abundance of D-sphingosine (DSP) and S1P in mouse plasma samples, extracts
257 were prepared and analyzed by TSQ Quantiva triple quadruple mass spectrometer coupled with a
258 Dionex UltiMate 3000 HPLC system (Thermo Fisher Scientific). Metabolites were extracted using ice cold
259 methanol with S1P-d7 as stable isotope internal standards. The lysates were vortexed, centrifuged at
260 17,000 g for 5 minutes at 4°C, and supernatants were transferred to clean autosampler injection vials
261 and 10 µL was injected for DSP/S1P analysis by liquid chromatography (LC)-MS. The mobile phase
262 A(MPA) is 0.1% Formic Acid in water. Mobile phase B(MPB) is 0.1% Formic Acid in acetonitrile.
263 Separations of S1P were achieved on an InertSustain Bio C18 HP, 3 µm, 100 x 2.1 mm column (GL
264 Sciences). The flow rate was 200 µL/min at 35 °C, and the gradient elution program was: initial 40%
265 MPB, increased to 60% MPB at 2 min, held at 60% MPB for 5 min, returned to initial conditions and
266 equilibrated for 4 min. The total run time was 11 min. The mass spectrometer was operated in the MRM
267 positive ion electrospray mode with the following transitions. S1P: m/z 380.3→264.2, DSP: m/z
268 300.3→252.3, S1P-d7 (IS): m/z 387.3 → 271.2, DSP-d7: 307.3 → 259.3. Raw data files were imported to
269 Trace Finder software (Thermo Fisher Scientific) for final analysis. The relative abundance of S1P was
270 normalized by internal standards.

271 **Analysis of gemcitabine by LC-MS**

272 KPC-4662-bearing mice treated with gemcitabine (Gem) or with exercise plus gemcitabine (Ex+Gem)
273 received a final i.v. dose of 25 mg/kg gemcitabine 1 hr prior to euthanization. Tumors were then
274 collected and frozen in liquid nitrogen for further analysis. To determine the relative abundance of
275 Gemcitabine (dFdC), extracts were prepared and analyzed by ultra-high-resolution mass spectrometry
276 (HRMS). Approximately 20-30 mgs of tissue were pulverized on liquid nitrogen, then homogenized with
277 Precellys Tissue Homogenizer (Bertin Corp.). Metabolites were extracted using 1 mL ice-cold 80/20 (v/v)
278 acetonitrile/water. Extracts were centrifuged at 17,000 g for 5 min at 4°C, and supernatants were
279 transferred to clean tubes, followed by evaporation to dryness under nitrogen. Dried extracts were
280 reconstituted in 50/50 (v/v) acetonitrile/water, and 10 µL was injected for analysis by liquid
281 chromatography (LC)-MS. LC mobile phase A (MPA) was 95/5 (v/v) water/acetonitrile containing 20mM
282 ammonium acetate and 20mM ammonium hydroxide (pH~9), and mobile phase B (MPB) was
283 acetonitrile. Vanquish LC system (Thermo Fisher Scientific) included a Xbridge BEH Amide column (3.5
284 µm particle size, 100 x 4.6 mm) with column compartment kept at 35°C. The autosampler tray was
285 chilled to 4°C. The mobile phase flow rate was 350 µL/min, and the gradient elution program was: 0-1
286 min, 85% MPB; 1-16 min, 85-5% MPB; 16-20 min, held at 5% MPB; 20-21 min, 5-85% MPB; 21-25 min,

287 re-equilibrate column at 85%MPB. The total run time was 25 min. Data were acquired using an Orbitrap
288 Exploris 240 Mass Spectrometer (Thermo Fisher Scientific) under ESI negative ionization mode at a
289 resolution of 120,000 with Select Ion Monitoring (SIM) mode. Raw data files were imported to Trace
290 Finder 5.1 software (Thermo Fisher Scientific) for final analysis. The relative abundance of each
291 metabolite was normalized by tissue weight. Sample numerosity for this analysis may vary from the
292 original mouse number due to the variable achievement of the final i.v. injections in mice that were very
293 ill.

294 **DNA isolation and amplification for S1PR1 EC-KO characterization**

295 The lungs of KPC-4662-bearing mice were harvested and immediately frozen in liquid nitrogen. DNA was
296 extracted with DNAzol reagent (Invitrogen, 10503-027) following manufacture's protocol. Briefly, lungs
297 were homogenized in DNAzol reagent, centrifuged to remove insoluble tissue fragments and RNA, and
298 DNA was precipitated and washed using ethanol 100% and 75%, respectively. DNA was then pelleted
299 and resuspended in 8 mM NaOH, 1M HEPES, pH 7.2, at a concentration of 0.2-0.3 µg/µl. To detect the
300 wild type (S1PR1 WT), knock-out (S1PR1 KO), and conditional alleles (S1PR1 loxP) by PCR the following
301 primers were used: P1, 5′ GAGCGGAGGAAGTTAAAAGTG; P2, 5′ CCTCCTAAGAGATTGCAGCAA. P1 and P2
302 amplify an approximately 250-bp fragment for the S1PR1 loxP allele and a 200-bp fragment for the
303 S1PR1 WT and S1PR1 KO alleles. To detect the recombined S1P1 allele, P1 and P3 (5′
304 GATCCTAAGGCAATGTCCTAGAATGGGACA) were used. P1 and P3 amplify a 200-bp fragment. When
305 primers P1, P2, and P3 were used in the same PCR reaction, the PCR products were digested with SacI
306 (Thermo Fisher Scientific, FD1133) prior to the electrophoresis, which converted the recombined S1P1
307 fragment to 180 bp.

308 **PDAC patient samples and exercise intervention**

309 We enrolled 151 patients with potentially resectable pancreatic cancer into a randomized study of a
310 prehabilitation home exercise intervention compared to usual care. The details of the trial have been
311 published[26]. Briefly, patients in the exercise program arm were recommended to engaged in at least 150
312 minutes of moderate-to-vigorous intensity aerobic exercise per week (self-monitored using Fitbit activity
313 trackers) and to perform at least 2 full-body strengthening exercise sessions per week (patients were
314 issued a set of resistance bands and video and paper guides). Patients in the usual care group were also
315 issued Fitbits to monitor their physical activity and received handouts with a full-body stretching guide
316 and information about the benefits of being physically active before surgery. Patients were enrolled in
317 this prehabilitation exercise program while receiving neoadjuvant chemotherapy and/or chemoradiation
318 and completed the intervention period at the time of preoperative restaging visits. Of note, 79 of the
319 151 patients (52%) completed neoadjuvant treatment and underwent pancreatectomy. There were no
320 significant differences in self-reported exercise minutes or Fitbit-measured physical activity between
321 study arms. Thus, for the study of tumor vasculature reported here, we combined all patients from both
322 arms for whom there were both surgical specimens and Fitbit data available (n=40). We calculated the
323 median number of minutes per week of "fairly active" (moderate), "very active" (vigorous) and "active"
324 minutes (the sum of "fairly active" and "very active" minutes which represents moderate-to-vigorous
325 physical activity) as recorded by Fitbit, then split patients into two groups: below, and above or equal
326 the median number of active minutes (130 minutes for active, and 66 minutes for fairly active and very
327 active). The analyses of the surgical tumor specimen for the 40 study patients are described above.

328 **Statistical analysis**

329 Statistical analysis was performed using SPSS software (IBM). Values in graphs are reported as mean
330 ±SEM, median with box and whiskers or Log_2 fold change. Shapiro-Wilk's normality test was performed
331 on datasets prior to statistical analysis. Nonparametric data were analyzed using an unpaired Mann–
332 Whitney t test and parametric data were analyzed using unpaired Student t test. For analysis including
333 more than 2 groups, the statistical comparisons were based on biological significance: Sed *vs* Ex 8 or Sed
334 *vs* Ex 16; Sed *vs* Ex or Gem *vs* Ex+Gem.

335 **Results**

336 **Aerobic exercise improves PDAC blood and lymphatic vasculature without impacting tumor mass and**
337 **metastasis**

338 To compare the impact of different aerobic exercise intensities on the vasculature of PDAC tumors in
339 mice, we exercised KPC-4662 tumor-bearing mice on treadmills at either 8 m/min or 16 m/min (~60% or
340 ~80% VO_2max, respectively[27]; **Fig. 1a**). Neither exercise intensity changed tumor weight or peritoneal
341 carcinomatosis as compared to sedentary mice (**Fig. 1b, c**). However, exercise at 16 m/min, but not at 8
342 m/min, increased the percentage of vessels with open lumens (23.2 vs 32.3%, p= 0.03) and elongated
343 vessels (2.3 vs 4.5%; p=0.017), without changing the total vessel number or vessel density (**Fig. 1d-h**),
344 compared to sedentary mice. Because exercise at 16 m/min effectively remodeled PDAC vasculature, we
345 used this intensity for further analysis. Tumors from mice that exercised at 16 m/min had more perfused
346 vessels than tumors from sedentary mice (p=0.033) (**Fig. 1l**) and significantly decreased vascular leakage
347 (**Fig. 1m**). Tumor hypoxia and the coverage of vessels by pericytes were not changed by exercise
348 (**Supplementary Fig. 2a-f**). Similar changes in vasculature were found in a second model of orthotopic
349 PDAC, Hy15549. In Hy 15549-bearing mice, exercise at 16 m/min did not affect the number of total
350 vessels, vessel density or elongated vessels (**Supplementary Figure 3a-d**), while it increased the
351 percentage of open lumens and decreased vascular leakage compared to tumors of sedentary mice
352 (**Supplementary Figure 3a, e-g**). Exercise did not change pericyte vessel coverage in Hy 15549 mice
353 (**Supplementary Fig. 3h, i**).

354 Because lymphatic vasculature contributes to fluid homeostasis and interstitial fluid pressure which
355 impacts drug delivery, lymphatic vessels were examined in the KPC-4662 model. Exercise significantly
356 increased the number of lymphatic vessels (**Fig. 1n, o**) relative to tumors from control mice. Exercise did
357 not change the percentage of lymphatic vessels with open lumens or elongated lymphatic vessels in
358 tumors (**Fig. 1n, p, q**).

359 **Aerobic exercise increases chemotherapy delivery and efficacy in mouse PDAC**

360 Blood and lymphatic vascular remodeling induced by exercise may increase the penetration of drugs
361 within the tumor and thus improve chemotherapy efficacy. To test this, we treated KPC-4662-bearing
362 mice with gemcitabine twice per week, with or without daily exercise at 16 m/min, for 3 weeks (**Fig. 2a**).
363 Exercise alone or in combination with gemcitabine increased the percentage of elongated vessels and
364 vessels with open lumens, but did not affect the total vessel number, vessel density or pericyte vessel
365 coverage as compared to sedentary animals (**Fig. 2b-f**; **Supplementary Fig. 4a, b**). Exercise with or
366 without gemcitabine also increased functional vasculature in tumors, as indicated by improved vessel
367 perfusion and decreased vascular leakage, as compared to sedentary controls or mice treated only with

368 gemcitabine (**Fig. 3a-c**). Consistent with improved vascular function leading to better delivery of
369 chemotherapy, exercise increased gemcitabine concentration within the tumor (32% increase in
370 exercised relative to gemcitabine alone treated mice; p= 0.025; **Fig. 3d**). The combination of exercise
371 and gemcitabine was more effective in reducing both tumor growth (p=0.028) and peritoneal metastasis
372 (62.5% reduction; p=0.002) as compared to gemcitabine alone (**Fig. 3e-g**).

373 **Aerobic exercise increases plasma S1P and activates S1PR1 on PDAC tumor endothelium**

374 To determine whether improved tumor vascular function is necessary for the improved chemotherapy
375 efficacy afforded by exercise, we first identified a key molecular mediator of the tumor vascular
376 response to exercise, S1PR1. Exercise did not change the expression of S1PR1 on tumor endothelial cells
377 (**Fig. 4a, b**). A reporter mouse model in which activation of S1PR1 is indicated by GFP expression (S1PR1-
378 GFP mice[24]) was utilized to measure S1PR1 signaling in tumor endothelium. The fidelity of the GFP
379 reporter in KPC-4662 tumors was confirmed by immunofluorescence (**Supplementary Fig. 5a**) and flow
380 cytometry on $CD31^{+}$ $CD45^{-}$ endothelial cells (**Supplementary Fig. 5b, c**). Exercise caused a significant
381 increase in S1PR1 activation in tumor endothelial cells compared to sedentary animals (**Fig. 4c**). Exercise
382 also increased the plasma levels of the S1PR1 ligand, S1P, and its precursor sphingosine (**Fig. 4d, e**).

383 **S1PR1 expression is necessary for the exercise-dependent improvement in vascular function and**
384 **chemotherapy efficacy**

385 Exercise increased tumor endothelial cell S1PR1 activation, and improved tumor vascular function and
386 chemotherapy efficacy. To define the role of S1PR1 in the exercise-induced remodeling of PDAC
387 vasculature, we used a mouse model of conditional endothelial specific deletion of S1PR1[20] (*S1pr1*$^{LoxP/LoxP}$
388 *Cdh5-Cre*-ER^{T2}; S1PR1 EKO). KPC-4662 tumors in S1PR1 EKO mice had increased tumor total endothelial
389 cell area, vessel number and density, and decreased open lumens as compared to control animals
390 (*S1pr1*$^{LoxP/LoxP}$ without *Cdh5-Cre*-ER^{T2} ; S1PR1 WT; **Supplementary Fig. 6a-e**). In addition, S1PR1
391 endothelial KO increased vascular leakage, without changing vascular perfusion or pericyte vessel
392 coverage in tumors (**Supplementary Fig. 6f-i**). Lymphatic endothelial cells also express *cdh5* and may be
393 affected by the *cdh5-cre* driven *s1pr1* deletion[28]. Tumors from S1PR1 EKO mice had decreased total
394 lymphatic vessels and percentage of elongated lymphatic vessels (**Supplementary Fig. 6l-n**). There was
395 no difference in tumor mass and peritoneal metastasis between S1PR1 EKO and S1PR1 WT mice
396 (**Supplementary Fig. 6o, p**).

397 Due to the activation of S1PR1 in tumor endothelium by exercise and the role of S1PR1 as an important
398 mediator of vascular maturation and function, we hypothesized that S1PR1 may be necessary for
399 improvements in tumor vascular function, and gemcitabine efficacy, by exercise. To test this hypothesis,
400 tumor-bearing S1PR1 EKO mice were exercised and treated with gemcitabine in the same way as S1PR1
401 WT mice (**Fig. 5a**). In contrast to S1PR1 WT mice, exercise did not remodel tumor vasculature or improve
402 tumor vascular function (**Fig. 5b-f; Fig 6 a-c**) and did not change pericyte coverage of vessels in S1PR1
403 EKO mice (**Supplementary Fig. 4c, d**). Exercise improved lymphatic vessel number and structure also in
404 the absence of endothelial S1PR1 (**Supplementary Fig. 6q-s**). Along with the loss of vascular remodeling
405 in S1PR1 EKO mice in response to exercise, the combination of exercise plus gemcitabine was ineffective
406 in increasing chemotherapy concentration and did not reduce tumor growth and peritoneal metastasis
407 as compared to gemcitabine alone in S1PR1 EKO mice (**Fig. 6d-e**). Taken together, these results suggest
408 that improved vascular function mediated by S1PR1 is necessary for improved gemcitabine efficacy
409 against PDAC in mice.

410 **Increased vigorous physical activity in PDAC patients remodels tumor vasculature and reduces tumor**
411 **vascular leakage**

412 We next validated the relevance of our findings in mice with PDAC tumors from patients who
413 participated in a study of home-based exercise during neoadjuvant therapy. Study design, clinical
414 demographics of participants, and primary outcomes were previously reported[26]. Participants were
415 randomized to enhanced usual care or to prescribed aerobic and resistance exercise. Tumor specimens
416 were obtained at the time of surgical resection for those patients who underwent surgery after
417 neoadjuvant therapy. Despite the exercise intervention, objectively measured weekly activity (by Fitbit)
418 and self-reported weekly moderate-to-strenuous physical activity minutes were not significantly
419 different between study arms. Due to of the lack of significant differences in physical activity between
420 the two arms, we also pooled the participants and divided them into two groups based on weekly fairly
421 active, active or very active minutes (moderate, moderate-to-vigorous and vigorous physical activity,
422 respectively; <median *vs* ≥median of average minutes/week) as measured by Fitbit. Tumors of patients
423 that performed more than the median number of minutes per week of vigorous physical activity showed
424 increased total vessel, vessel density, number of vessels with open lumens and elongated vessels (**Fig.**
425 **7a-e**). In the same patients, there was a significant decrease in tumor vascular leakage as indicated by
426 albumin. Grouping the patients by experimental study arms or as above or below the median of weekly
427 fairly active and active minutes did not show differences between groups, except for the increased
428 number of vessels with open lumens in patients above the median number of active minutes per week
429 (**Supplementary Fig. 7**).

430 **Discussion**

431 Despite the advancements made in therapeutic approaches against PDAC, the majority of patients have
432 disease that continues to progress on therapy, leading to low survival rates[29]. Chemotherapy efficacy
433 against PDAC is blunted in part by poor delivery to the tumor cells. Drug delivery to the tumor is
434 impeded by dysfunctional, sparse blood and lymphatic vasculature[30], by the solid stress imposed by
435 cancer cell growth, and by the excessive deposition of extracellular matrix that characterizes PDAC[31]. In
436 this study, we demonstrated that aerobic exercise is an effective tool for improving chemotherapy
437 delivery and efficacy against pancreatic tumors and peritoneal metastasis in mice. These effects were
438 mediated by tumor vascular normalization via S1P – S1PR1 signaling. When blood vessels were unable
439 to remodel in response to exercise, the added benefit of exercise for chemotherapy efficacy was lost.
440 Evaluation of surgically resected PDAC from patients who participated in an exercise intervention during
441 neoadjuvant therapy indicates that exercise may be a useful clinical tool to support microenvironment
442 changes that allow better drug access to the tumor.

443 We did not find an effect of exercise without chemotherapy on tumor growth or metastasis. This is in
444 contrast to other preclinical studies which found that exercise alone reduced tumor growth[13,32–35]. The
445 effect of exercise on tumor growth varies by the tumor type, tumor location, exercise protocol, and the
446 time of exercise initiation relative to tumor inoculation. Despite no effect of exercise alone on tumor
447 growth, exercise combined with gemcitabine reduced the primary tumor growth and peritoneal
448 metastasis more than gemcitabine alone. Exercise decreased tumor vessel permeability and increased
449 gemcitabine concentration within tumors, consistent with reduced metastatic spread related to better
450 drug delivery and/or an improved physical barrier to tumor cell extravasation. Exercise also increased
451 the number of lymphatic vessels in the tumor. Although increased lymphatic vessels may have the

452 potential to increase the dissemination of tumor cells[36–39], there was no difference in peritoneal
453 spreading of PDAC in exercised mice in the absence of chemotherapy. When delivered with
454 gemcitabine, exercise reduced peritoneal metastasis of PDAC in mice. The reduction of PDAC metastasis
455 is a novel finding of critical importance because when patients develop metastatic disease during
456 neoadjuvant therapy, they become ineligible for surgery. Thus, our work supports a potential role for
457 exercise during neoadjuvant therapy to increase the chance of curative surgery.

458 Aerobic exercise has been shown to improve anti-cancer therapy in different animal models[11,12,14,33,40–42].
459 While some studies have suggested that this is due to improved blood vessel function and one has
460 demonstrated a role for Thrombospondin-1 in the tumor endothelial response to exercise[11], the specific
461 regulation of tumor vasculature by exercise and the relevance of these changes remain enigmatic. We
462 found that exercise increased S1PR1 activation on tumor endothelium, consistent with the known
463 function of S1PR1 in promoting improved tumor vascular structure and function[23]. Endothelial cell-
464 specific *s1pr1* deletion prevented the exercise induced improvements of tumor blood vessels but not
465 lymphatic vessels, indicating that exercise-induced blood, but not lymphatic, vessel remodeling is
466 dependent on S1PR1. Exercise did not increase gemcitabine concentration and efficacy in S1PR1 EKO
467 mice, indicating a causal relationship of improved tumor blood vessel function leading to increased
468 chemotherapy delivery and efficacy. Because the effects of exercise in lymphatic vessels were not
469 different in S1PR1 EKO relative to S1PR1 WT mice, we conclude that an improvement in blood vessels
470 alone is sufficient for exercise-induced increased chemotherapy delivery and efficacy. In summary, the
471 present study defined S1PR1 as a necessary mediator of the PDAC vascular remodeling and increased
472 chemotherapy efficacy upon exercise.

473 Exercise is a feasible and effective tool to improve physical fitness and quality of life in patients
474 undergoing treatment for PDAC[26,43,44]. Additionally, improved tumor vessel maturity and function
475 correlates with better outcomes for patients with PDAC who receive neoadjuvant chemotherapy[45].
476 Here, we demonstrated in mice that exercise improved blood vessel function, improved chemotherapy
477 efficacy, and decreased metastasis. We also validated the relationship between vigorous physical
478 activity and tumor vasculature in patient PDAC using a cohort from a clinical study in which patients
479 underwent an exercise program during neoadjuvant therapy. The limitations of this clinical study include
480 the inaccuracy of the activity tracker to measure the prescribed exercise program rather than day-to-day
481 activity, and the lack of difference in self-reported exercise minutes or Fitbit-measured physical activity
482 between study arms, leading us to divide the patients into groups based on the median of weekly Fitbit-
483 measured activity minutes. Taken together, our data in mice and in patients suggests that exercise may
484 be beneficial for increasing the efficacy of anti-cancer treatment and survival.

485 **Acknowledgments**

486 R.B., J.L. and K.S. were supported by Cancer Prevention and Research Institute of Texas (CPRIT, grant
487 RP190256). The clinical trial was supported by a generous gift from the Wyck Knox Family Foundation.
488 P.T. was supported by CPRIT, grant RP210028. S.P. was supported by the Pauline Altman-Goldstein
489 Foundation Discovery Fellowship.

490 **Author Contributions**

491 R.B. contributed to conceptualization, design, data acquisition, data curation, formal analysis, validation,
492 investigation, methodology, writing–original draft, writing–review and editing. S.P., J.L. and H.P.

493 contributed to data acquisition, formal analysis, data curation, writing–review and editing. P.T. and K.H.
494 contributed to formal analysis, data curation, writing–review and editing. G.L. contributed to formal
495 analysis and data curation. H.S. and B.G. contributed to conceptualization, writing–review and editing.
496 A.N., N.P., M.H.K., M.P. and F.M. conducted the clinical trial and provided access to patient samples.
497 R.W. contributed to data curation, writing–review and editing. T.L. and P.L.L. contributed to the analysis
498 and writing–review and editing. K.S. contributed to conceptualization, resources, data curation, formal
499 analysis, supervision, funding acquisition, writing–original draft, project administration, writing–review
500 and editing.

501 **Competing interests**

502 The authors declare no competing interests.

503 **Materials & correspondence**

504 Keri Schadler, PhD. The University of Texas MD Anderson Cancer Center, 1515 Holcombe Blvd, Houston,
505 TX 77030. Phone: 713-794-1035; Fax: 713-563-5604; E-mail: klschadl@mdanderson.org

506 **Figure Legends**

507 **Supplementary Figure 1. S1PR1 EKO genotype verification, tumor volume calculation and**
508 **experimental scheme. a** Lung DNA characterization from *S1pr1*$^{flox/flox}$, *S1pr1*$^{flox/flox}$ Cdh5-Cre-ER^{T2} (S1PR1
509 EKO) and wild-type (WT) mice. The combination of primers used amplified different products: 250 bp
510 S1PR1 loxP; 200 bp S1PR1 WT or KO; 180 bp SacI digested S1PR1 KO fragment ΔEx2. All mice were
511 treated with tamoxifen as described in methods, except for WT. **b** Representative images of S1PR1
512 (green) immunofluorescence staining in CD31^{+} (red) vessels in S1PR1 WT (*S1pr1*$^{flox/flox}$) and S1PR1 EKO
513 mice. Scale bar, 50 µm. **c** Representative tumor ultrasound pictures. For tumor volume calculation, two
514 different pictures of a single tumor were acquired by ultrasound. The pictures were obtained taking two
515 tangential ultrasound images along the transverse and longitudinal planes. Tumor volume was
516 calculated by the formula 4/3πABC, where A, B and C are the measured diameters of each tumor. Values
517 were expressed as mm^3. **d** Exercise, acclimatization and ultrasound (US) experimental scheme for 8 and
518 16 meters/minute (m/min) exercise protocols.

519 **Figure 1. Aerobic exercise alone does not impact tumor mass or metastasis, but it improves tumor**
520 **blood and lymphatic vasculature at higher intensity. a** Experimental scheme of aerobic exercise
521 training, including orthotopic injection of KPC-4662 cells, exercise acclimatization, exercise phase, and
522 euthanization. **b** Tumor weights in grams (g). **c** Peritoneal carcinomatosis index (PCI) expressed as total
523 metastasis score for each animal. **d-h** Representative images of tumor vascular structure. Vasculature
524 was evaluated using immunofluorescence staining for CD31 (green) with DAPI (blue) counterstaining
525 and quantified on five to nine sections per tumor. **I-m** Representative images of vessel perfusion and
526 vascular leakage. Vessel perfusion was calculated as the ratio between lectin (red):CD31 (green)
527 immunofluorescence signal. Vascular leakage was calculated as the ratio between albumin
528 (magenta):CD31 (green) immunofluorescence signal. **n-q** Representative images of tumor lymphatic
529 vessel structure. Lymphatic vessel structure was evaluated using LYVE-1 (green) immunofluorescence
530 staining with DAPI (blue) counterstaining. Scale bar, 100µm. For all graphs, each point indicates one
531 tumor. Bars indicate mean ± SEM. * $p<0.05$ relative to Sed.

532 **Supplementary Figure 2**. **Exercise does not impact hypoxia or pericyte vessel coverage in tumors**. **a, b**
533 Representative images of tumor hypoxia. Tumor hypoxia was calculated as the ratio between
534 hypoxyprobe (green) immunofluorescence signal and the number of DAPI$^+$ (blue) nuclei. Scale bar, 1
535 mm. **c-f** Representative images of perycite vessel coverage. Pericyte vessel coverage was evaluated by
536 analyzing the percentage of colocalization between αSMA$^+$, desmin$^+$ or NG2$^+$ pericyte (magenta) and
537 CD31$^+$ (green) vessels, with DAPI (blue) counterstaining. Scale bar, 100µm. For all graphs, each point
538 indicates one tumor. Bars indicate mean ± SEM.

539 **Supplementary Figure 3. Exercise at 16 m/min remodels vascular structure and decreases vascular**
540 **leakage in Hy 15549 tumors. a-e** Representative images of tumor vascular structure. Tumor vascular
541 structure was evaluated using CD31 (green) immunofluorescence staining with DAPI (blue)
542 counterstaining. **f, g** Representative images of vascular leakage. Vascular leakage was calculated as the
543 ratio between albumin (magenta):CD31 (green) immunofluorescence signal. **h, i** Pericyte vessel
544 coverage was evaluated by analyzing the percentage of colocalization between markers αSMA$^+$ or NG2$^+$
545 pericyte (magenta) and CD31$^+$ (green) vessels, with DAPI (blue) counterstaining. Scale bar, 100µm. For all
546 graphs, each point indicates one tumor. Bars indicate mean ± SEM. * $p<0.05$ relative to Sed.

547 **Figure 2. Exercise with or without chemotherapy improves tumor vascular structure. a** Experimental
548 scheme of aerobic exercise training, including KPC-4662 cells orthotopic injection, exercise
549 acclimatization, gemcitabine treatment schedule and euthanization. **b-f** Representative images of tumor
550 vascular structure. Tumor vascular structure was evaluated using CD31 (green) immunofluorescence
551 staining with DAPI (blue) counterstaining. Scale bar, 100µm. For all graphs, each point indicates one
552 tumor. Bars indicate mean ± SEM. ** $p<0.01$; *** $p<0.001$ relative to Sed or Gem.

553 **Figure 3. Exercise with or without gemcitabine improves vascular function, increases chemotherapy**
554 **delivery and efficacy, and reduces peritoneal metastasis. a-c** Representative images of vessel perfusion
555 and vascular leakage. Vessel perfusion was calculated as the ratio between lectin (red):CD31 (green)
556 immunofluorescence signal. Vascular leakage was calculated as the ratio between albumin
557 (magenta):CD31 (green) immunofluorescence signal. Vascular leakage expressed as the ratio between
558 albumin (purple):CD31 (green) immunofluorescence signal. Scale bar, 100µm. **d** Gemcitabine (dFdC)
559 concentration measured by LC-MS and expressed as Log_2 fold change *vs* Gem. **e, f** Representative
560 ultrasound pictures of tumors showing difference in tumor area (dotted circle). Tumor weight in grams
561 (g). **g** Peritoneal carcinomatosis index (PCI) expressed as total metastasis score for each animal. For all
562 graphs, each point indicates one tumor. Bars indicate mean ± SEM, except for dFdC concentration
563 expressed as median with box and whiskers. * $p<0.05$; ** $p<0.01$ relative to Sed or Gem.

564 **Supplementary Figure 4. Exercise with or without chemotherapy does not affect pericyte vessel**
565 **coverage in S1PR1 WT or EKO mice. a-d** Pericyte vessel coverage was evaluated by analyzing the
566 percentage of colocalization between αSMA$^+$ or NG2$^+$ pericyte (magenta) and CD31$^+$ (green) vessels, with
567 DAPI (blue) counterstaining. Scale bar, 100µm. Data are expressed as mean ± SEM.

568 **Supplementary Figure 5. S1PR1-GFP reporter mouse verification and flow cytometry gating strategy. a**
569 Representative image of KPC-4662 tumors from H2B-GFP (control) or S1PR1-GFP mice; DAPI$^+$ (blue) GFP$^+$
570 (green) signal in CD31$^+$ (red) vessels. White arrows indicate GFP-positive endothelial cell nuclei. Scale
571 bar, 100µm. **b** Gating strategy for the flow cytometry analysis of S1PR1 activation in tumor endothelial
572 cells of S1PR1-GFP reporter mice. Single cell suspensions are gated for CD31$^+$ and CD45$^-$ cells for the

573 identification of vascular endothelial cells. **c** Representative histogram showing the GFP fluorescence
574 intensity for H2B-GFP (red) and S1PR1-GFP (green) tumors.

575 **Figure 4. Aerobic exercise increases S1PR1 activity in tumor endothelial cells and plasma sphingosine**
576 **and S1P, without affecting tumor endothelial cell S1PR1 expression. a, b** Representative pictures of
577 S1PR1 staining. S1PR1 tumor endothelial expression was analyzed by immunofluorescence and
578 expressed as percentage colocalization between S1PR1 (red) and CD31 (green) immunofluorescence
579 signal. Scale bar, 100µm. **c** Endothelial cell S1PR1 activation was analyzed by measuring GFP mean
580 fluorescence intensity (MFI) by flow cytometry in $CD31^+$ $CD45^-$ cells. **d, e** Plasma sphingosine-1-
581 phosphate (S1P) and sphingosine were analyzed by LC-MS and expressed as nM. For
582 immunofluorescence and flow cytometry data graphs, each point indicates one tumor, bars indicate
583 mean ± SEM. For LC-MS data, each point represents one mouse and summary data is shown as box and
584 whiskers with median. * $p<0.05$ relative to Sed or Gem.

585 **Supplementary Figure 6. S1PR1 EKO alters blood and lymphatic vessel structure and vascular leakage.**
586 **a** Tumor CD31 immunofluorescence area was expressed as arbitrary units and evaluated in tile scan
587 tumor sections. **b-e** Tumor vascular structure was analyzed using CD31 immunofluorescence staining
588 with DAPI counterstaining. **f** Vessel perfusion was calculated as the ratio between lectin (red):CD31
589 (green) immunofluorescence signal. **g** Vascular leakage was calculated as the ratio between albumin
590 (magenta):CD31 (green) immunofluorescence signal. **h-i** Pericyte vessel coverage was evaluated by
591 analyzing the percentage of colocalization between αSMA^+ or $NG2^+$ pericyte and $CD31^+$ vessels, with
592 DAPI counterstaining. **l-n, q-s** Lymphatic vessel structure was evaluated using LYVE-1
593 immunofluorescence staining with DAPI counterstaining in S1PR1 WT *vs* EKO mice or S1PR1 KO Sed *vs*
594 Ex. **o** Tumor weight was expressed as grams (g). **p** Peritoneal carcinomatosis index (PCI) was expressed
595 as total metastasis score for each animal. For all graphs, each point indicates one tumor. Bars indicate
596 mean ± SEM. * $p<0.05$; ** $p<0.01$ relative to S1PR1 WT.

597 **Figure 5. S1PR1 EKO blunts the exercise-induced improvements of tumor vascular structure. a**
598 Experimental scheme of aerobic exercise training, including KPC-4662 cells orthotopic injection, exercise
599 acclimatization, gemcitabine treatment schedule and euthanization in S1PR1 EKO mice. **b-f**
600 Representative pictures of S1PR1 staining. Tumor vascular structure was evaluated using CD31 (green)
601 immunofluorescence staining with DAPI (blue) counterstaining. Scale bar, 100µm. For all graphs, each
602 point indicates one tumor. Bars indicate mean ± SEM.

603 **Figure 6. S1PR1 EKO blunts the exercise-induced improvements in tumor vascular function,**
604 **chemotherapy delivery and efficacy and peritoneal metastasis. a-c** Representative images of vessel
605 perfusion and vascular leakage. Vessel perfusion was calculated as the ratio between lectin (red):CD31
606 (green) immunofluorescence signal. Vascular leakage was calculated as the ratio between albumin
607 (magenta):CD31 (green) immunofluorescence signal. Scale bar, 100µm. **d** Gemcitabine (dFdC)
608 concentration measured by LC-MS and expressed as Log_2 fold change *vs* Gem. **e, f** Representative
609 ultrasound pictures of tumors showing difference in tumor area (dotted circle). Tumor weight in grams
610 (g). **g** Peritoneal carcinomatosis index (PCI) expressed as total metastasis score for each animal. For all
611 graphs, each point indicates one tumor. Bars indicate mean ± SEM, except for dFdC concentration
612 expressed as median with box and whiskers.

613 **Figure 7. Exercise during neoadjuvant therapy remodeled tumor vasculature and decreased tumor**
614 **vascular leakage in PDAC patients.** Patients were divided in two groups based on the median number of

615 minutes of very active physical activity performed weekly, as tracked by Fitbit (<66 *vs* ≥66 minutes).
616 Tumors obtained during surgical resection were assessed by immunofluorescent staining. **a-e**
617 Representative images of tumor vascular structure. Tumor vascular structure was evaluated using CD31
618 (red) immunofluorescence staining with DAPI (blue) counterstaining. **f, g** Representative images of
619 vascular leakage. Vascular leakage was calculated as the ratio between albumin (magenta):CD31 (green)
620 immunofluorescence signal. Scale bar, 100µm. Bars indicate mean ± SEM. p values are shown above
621 bars.

622 **Supplementary Figure 7. There are no significant changes in tumor vascular structure and tumor**
623 **vascular leakage when patient samples are divided by study arms, or by the median of weekly fairly**
624 **active or active minutes. a-n** Tumor vascular structure was evaluated using CD31 (red)
625 immunofluorescence staining with DAPI (blue) counterstaining. **o, q** Vascular leakage was calculated as
626 the ratio between albumin (magenta):CD31 (green) immunofluorescence signal. Scale bar, 100µm.
627 Patients were divided in two groups based on arms (Arm A = Usual Care and Arm B = Exercise; or based
628 on the median number of minutes of fairly active or active physical activity performed weekly (<66 *vs*
629 ≥66 minutes and <130 *vs* ≥130 minutes, respectively). Bars indicate mean ± SEM. p values are shown
630 above bars.

631

632 **References**

633 1. Halbrook, C. J., Lyssiotis, C. A., Pasca di Magliano, M. & Maitra, A. Pancreatic cancer: Advances
634 and challenges. *Cell* **186**, 1729–1754 (2023).

635 2. Hosein, A. N., Dougan, S. K., Aguirre, A. J. & Maitra, A. Translational advances in pancreatic ductal
636 adenocarcinoma therapy. *Nat Cancer* **3**, 272–286 (2022).

637 3. Neoptolemos, J. P. *et al.* Therapeutic developments in pancreatic cancer: Current and future
638 perspectives. *Nat Rev Gastroenterol Hepatol* **15**, 333–348 (2018).

639 4. Hosein, A. N., Brekken, R. A. & Maitra, A. Pancreatic cancer stroma: an update on therapeutic
640 targeting strategies. *Nat Rev Gastroenterol Hepatol* **17**, 487–505 (2020).

641 5. Sherman, M. H. & Beatty, G. L. Tumor Microenvironment in Pancreatic Cancer Pathogenesis and
642 Therapeutic Resistance. *Annual Review of Pathology: Mechanisms of Disease* **18**, 123–148 (2023).

643 6. Di Maggio, F. *et al.* Pancreatic stellate cells regulate blood vessel density in the stroma of
644 pancreatic ductal adenocarcinoma. *Pancreatology* **16**, 995–1004 (2016).

645 7. Chauhan, V. P. *et al.* Compression of Pancreatic Tumor Blood Vessels by Hyaluronan Is Caused by
646 Solid Stress and Not Interstitial Fluid Pressure. *Cancer Cell* **26**, 14–15 (2014).

647 8. Dieterich, L. C., Tacconi, C., Ducoli, L. & Detmar, M. Lymphatic Vessels in Cancer. *Physiol Rev* **102**,
648 1837–1879 (2022).

649 9. Longo, V. *et al.* Angiogenesis in pancreatic ductal adenocarcinoma: A controversial issue.
650 *Oncotarget* **7**, 58649–58658 (2016).

651 10. Wu, M. *et al.* The effect of interstitial pressure on tumor growth: Coupling with the blood and
652 lymphatic vascular systems. *J Theor Biol* **320**, 131–151 (2013).

653 11. Schadler, K. L. *et al.* Tumor vessel normalization after aerobic exercise enhances
654 chemotherapeutic efficacy. *Oncotarget* **7**, 65429–65440 (2016).

655 12. Florez Bedoya, C. A. *et al.* Exercise during preoperative therapy increases tumor vascularity in
656 pancreatic tumor patients. *Sci Rep* **9**, 1–8 (2019).

657 13. Savage, H. *et al.* Aerobic Exercise Alters the Melanoma Microenvironment and Modulates ERK5
658 S496 Phosphorylation. *Cancer Immunol Res* **1**, OF1–OF16 (2023).

659 14. Morrell, M. B. G. *et al.* Vascular modulation through exercise improves chemotherapy efficacy in
660 Ewing sarcoma. *Pediatr Blood Cancer* **66**, 1–11 (2019).

661 15. Savage, H. *et al.* Aerobic Exercise Alters the Melanoma Microenvironment and Modulates ERK5
662 S496 Phosphorylation. *Cancer Immunol Res* **1**, OF1–OF16 (2023).

663 16. Blaho, V. A. & Hla, T. An update on the biology of sphingosine 1-phosphate receptors. *J Lipid Res*
664 **55**, 1596–1608 (2014).

665 17. Prager, B., Spampinato, S. F. & Ransohoff, R. M. Sphingosine 1-phosphate signaling at the blood-
666 brain barrier. *Trends Mol Med* **21**, 354–363 (2015).

667 18. Paik, J. H. *et al.* Sphingosine 1-phosphate receptor regulation of N-cadherin mediates vascular
668 stabilization. *Genes Dev* **18**, 2392–2403 (2004).

669 19. Liu, Y. *et al.* Edg-1, the G protein-coupled receptor for sphingosine-1-phosphate, is essential for
670 vascular maturation. *J Clin Invest* **106**, 951–961 (2000).

671 20. Allende, M. L., Yamashita, T. & Proia, R. L. G-protein-coupled receptor S1P1 acts within
672 endothelial cells to regulate vascular maturation. *Blood* **102**, 3665–3667 (2003).

673 21. Jung, B. *et al.* Flow-Regulated Endothelial S1P Receptor-1 Signaling Sustains Vascular
674 Development. *Dev Cell* **23**, 600–610 (2012).

675 22. Marmonti, E. *et al.* Modulating sphingosine-1-phosphate receptors to improve chemotherapy
676 efficacy against Ewing sarcoma. *Int J Cancer* **2**, 1–10 (2020).

677 23. Cartier, A., Leigh, T., Liu, C. H. & Hla, T. Endothelial sphingosine 1-phosphate receptors promote
678 vascular normalization and antitumor therapy. *Proc Natl Acad Sci U S A* **117**, 3157–3166 (2020).

679 24. Kono, M. *et al.* Sphingosine-1-phosphate receptor 1 reporter mice reveal receptor activation sites
680 in vivo. *Journal of Clinical Investigation* **124**, 2076–2086 (2014).

681 25. Bastiaenen, V. P. *et al.* A mouse model for peritoneal metastases of colorectal origin
682 recapitulates patient heterogeneity. *Laboratory Investigation* **100**, 1465–1474 (2020).

683 26. Ngo-Huang, A. T. *et al.* Effects of a Pragmatic Home-based Exercise Program Concurrent With
684 Neoadjuvant Therapy on Physical Function of Patients With Pancreatic Cancer: The PancFit
685 Randomized Clinical Trial. *Ann Surg* **278**, 22–30 (2023).

686 27. Schefer, V. & Talan, M. I. Oxygen consumption in adult and aged C57BL/6J mice during acute
687 treadmill exercise of different intensity. *Exp Gerontol* **31**, 387–392 (1996).

688 28. Nakashima, B. J. & Hong, Y. K. VE-Cadherin: A Critical Sticking Point for Lymphatic System
689 Maintenance Role of VE-Cadherin in Lymphatic Maintenance. *Circ Res* **130**, 24–26 (2022).

690 29. Quiñonero, F. *et al.* The challenge of drug resistance in pancreatic ductal adenocarcinoma: a
691 current overview. *Cancer Biol Med* **16**, 688–699 (2019).

692 30. Wu, M. *et al.* The effect of interstitial pressure on tumor growth: Coupling with the blood and
693 lymphatic vascular systems. *J Theor Biol* **320**, 131–151 (2013).

694 31. Adiseshaiah, P. P., Crist, R. M., Hook, S. S. & McNeil, S. E. Nanomedicine strategies to overcome
695 the pathophysiological barriers of pancreatic cancer. *Nat Rev Clin Oncol* **13**, 750–765 (2016).

696 32. Hojman, P., Gehl, J., Christensen, J. F. & Pedersen, B. K. Molecular Mechanisms Linking Exercise
697 to Cancer Prevention and Treatment. *Cell Metab* **27**, 10–21 (2017).

698 33. Kurz, E. *et al.* Exercise-induced engagement of the IL-15/IL-15Rα axis promotes anti-tumor
699 immunity in pancreatic cancer. *Cancer Cell* **40**, 720-737.e5 (2022).

700 34. Hsueh, H. Y. *et al.* A review of physical activity in pancreatic ductal adenocarcinoma:
701 Epidemiology, intervention, animal models, and clinical trials. *Pancreatology* **22**, 98–111 (2022).

702 35. Pedersen, L. *et al.* Voluntary Running Suppresses Tumor Growth through Epinephrine- and IL-6-
703 Dependent NK Cell Mobilization and Redistribution. *Cell Metab* **23**, 554–562 (2016).

704 36. Karaman, S. & Detmar, M. Mechanisms of lymphatic metastasis. *Journal of Clinical Investigation*
705 **124**, 922–928 (2014).

706 37. Shen, C. N. *et al.* Lymphatic vessel remodeling and invasion in pancreatic cancer progression.
707 *EBioMedicine* **47**, 98–113 (2019).

708 38. Fink, D. M., Steele, M. M. & Hollingsworth, M. A. The lymphatic system and pancreatic cancer.
709 *Cancer Lett* **381**, 217–236 (2016).

710 39. Sherman, M. H. & Beatty, G. L. Tumor Microenvironment in Pancreatic Cancer Pathogenesis and
711 Therapeutic Resistance. *Annual Review of Pathology: Mechanisms of Disease* **18**, 123–148 (2023).

712 40. Betof, A. S. *et al.* Modulation of murine breast tumor vascularity, hypoxia, and chemotherapeutic
713 response by exercise. *J Natl Cancer Inst* **107**, 1–5 (2015).

714 41. Dufresne, S. *et al.* Exercise training improves radiotherapy efficiency in a murine model of
715 prostate cancer. *FASEB Journal* **34**, 4984–4996 (2020).

716 42. Wennerberg, E. *et al.* Exercise reduces immune suppression and breast cancer progression in a
717 preclinical model. *Oncotarget* **11**, 452–461 (2020).

718 43. Ngo-Huang, A. *et al.* Home-Based Exercise Prehabilitation During Preoperative Treatment for
719 Pancreatic Cancer Is Associated With Improvement in Physical Function and Quality of Life. *Integr*
720 *Cancer Ther* **18**, 1534735419894061 (2019).

721 44. Gupta, P., Hodgman, C. F., Schadler, K. L. & LaVoy, E. C. Effect of exercise on pancreatic cancer
722 patients during treatment: a scoping review of the literature. *Supportive Care in Cancer* **30**, 5669–
723 5690 (2022).

724 45. Katsuta, E. *et al.* Pancreatic adenocarcinomas with mature blood vessels have better overall
725 survival. *Sci Rep* **9**, 1–11 (2019).

726

Figure 1

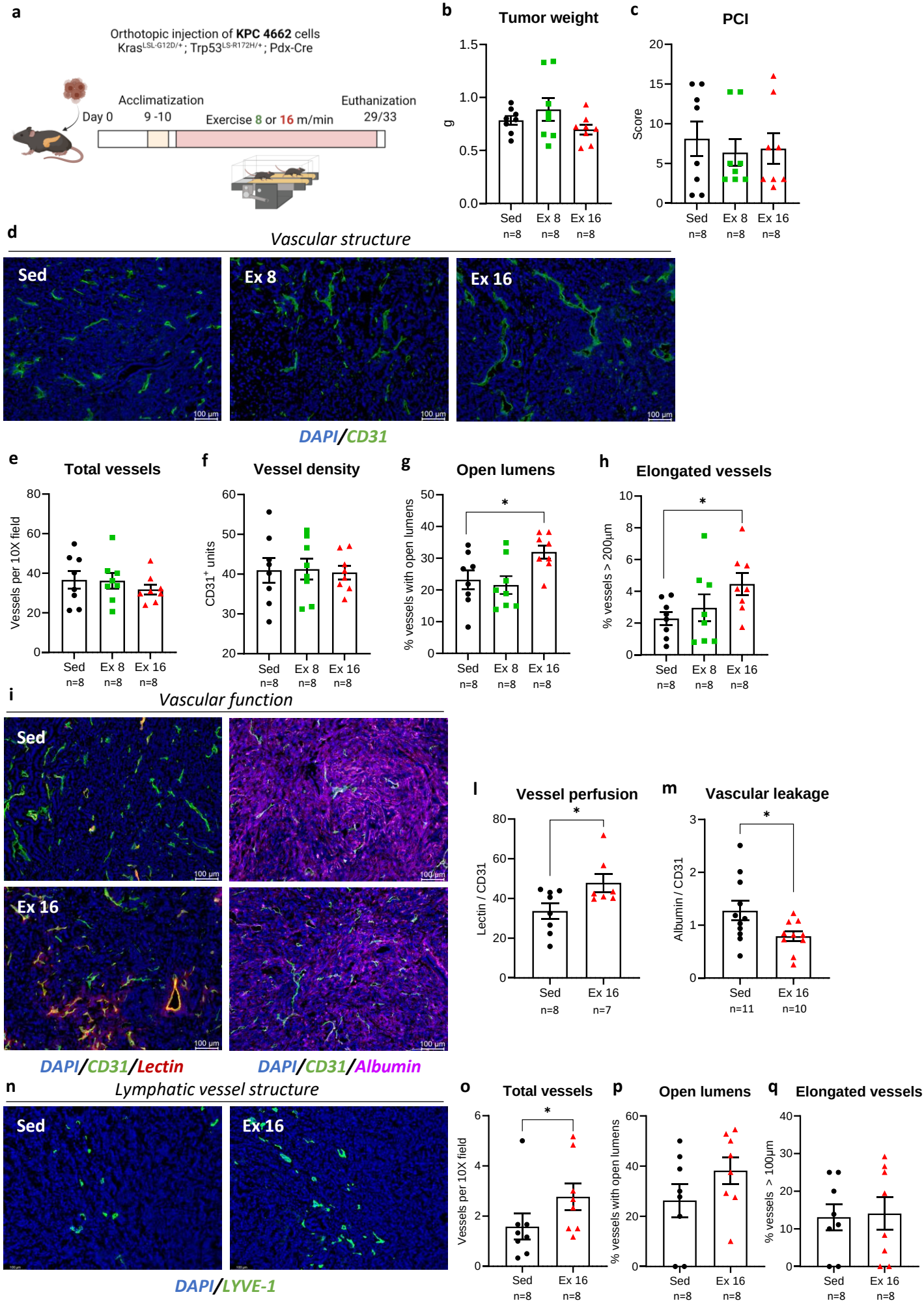
a
Orthotopic injection of KPC 4662 cells
Kras LSL-G12D/+; Trp53 LS-R172H/+; Pdx-Cre
Day 0
Acclimatization
9 -10
Exercise 8 or 16 m/min
Euthanization
29/33
b
Tumor weight
g
Sed n=8
Ex 8 n=8
Ex 16 n=8
c
PCI
Score
d
Vascular structure
Sed
Ex 8
Ex 16
100 µm
DAPI/CD31
e
Total vessels
Vessels per 10X field
f
Vessel density
CD31+ units
g
Open lumens
% vessels with open lumens
h
Elongated vessels
% vessels > 200µm
i
Vascular function
Sed
Ex 16
DAPI/CD31/Lectin
DAPI/CD31/Albumin
l
Vessel perfusion
Lectin / CD31
Ex 16 n=7
m
Vascular leakage
Albumin / CD31
Sed n=11
Ex 16 n=10
n
Lymphatic vessel structure
DAPI/LYVE-1
o
Total vessels
p
Open lumens
q
Elongated vessels
% vessels > 100µm

Figure 2

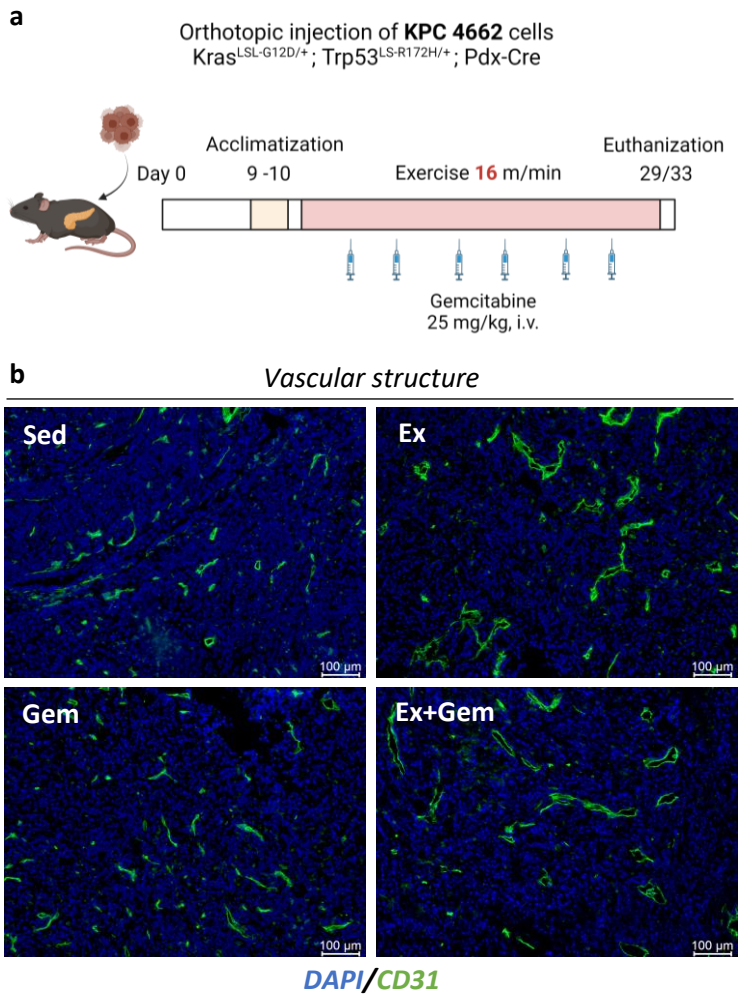
a
Orthotopic injection of KPC 4662 cells
Kras LSL-G12D/+ ; Trp53 LS-R172H/+ ; Pdx-Cre
Day 0
Acclimatization
9 -10
Exercise 16 m/min
Euthanization
29/33
Gemcitabine
25 mg/kg, i.v.
b
Vascular structure
Sed
Ex
Gem
Ex+Gem
100 µm
DAPI/CD31

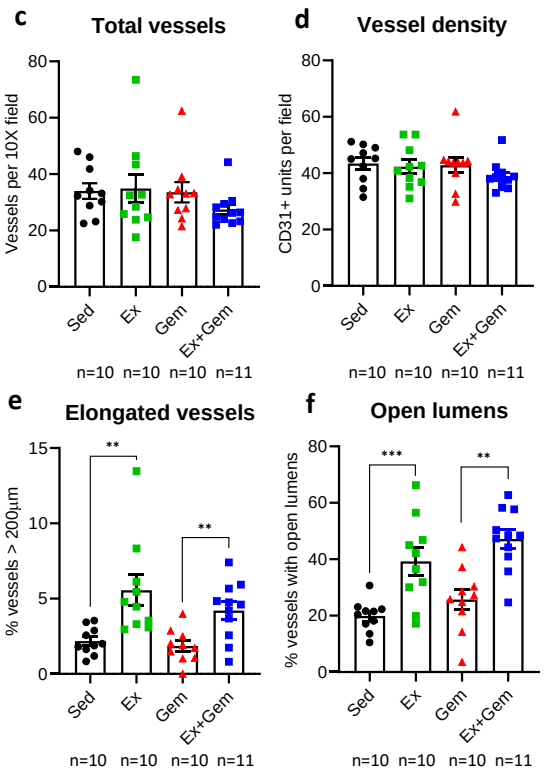
c
Total vessels
Vessels per 10X field
d
Vessel density
CD31+ units per field
e
Elongated vessels
% vessels > 200µm
f
Open lumens
% vessels with open lumens
Sed
Ex
Gem
Ex+Gem
n=10 n=10 n=10 n=11
**
***

Figure 3

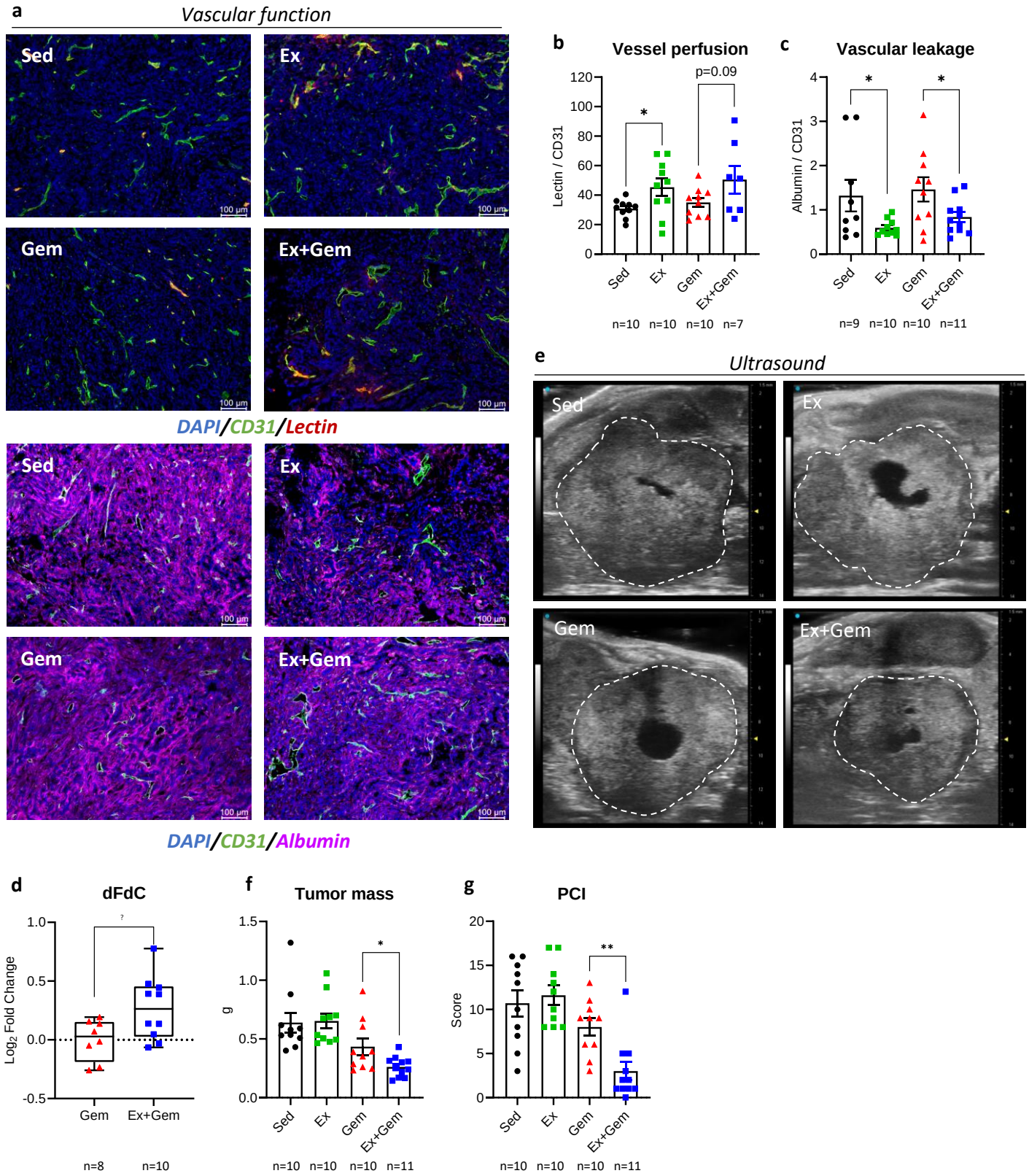
a
Vascular function
Sed
Ex
Gem
Ex+Gem
100 µm
DAPI/CD31/Lectin
DAPI/CD31/Albumin
b
Vessel perfusion
Lectin / CD31
p=0.09
*
Sed Ex Gem Ex+Gem
n=10 n=10 n=10 n=7
c
Vascular leakage
Albumin / CD31
*
*
Sed Ex Gem Ex+Gem
n=9 n=10 n=10 n=11
e
Ultrasound
Sed
Ex
Gem
Ex+Gem
d
dFdC
Log2 Fold Change
?
Gem Ex+Gem
n=8 n=10
f
Tumor mass
g
*
Sed Ex Gem Ex+Gem
n=10 n=10 n=10 n=11
g
PCI
Score
**
Sed Ex Gem Ex+Gem
n=10 n=10 n=10 n=11

Figure 4

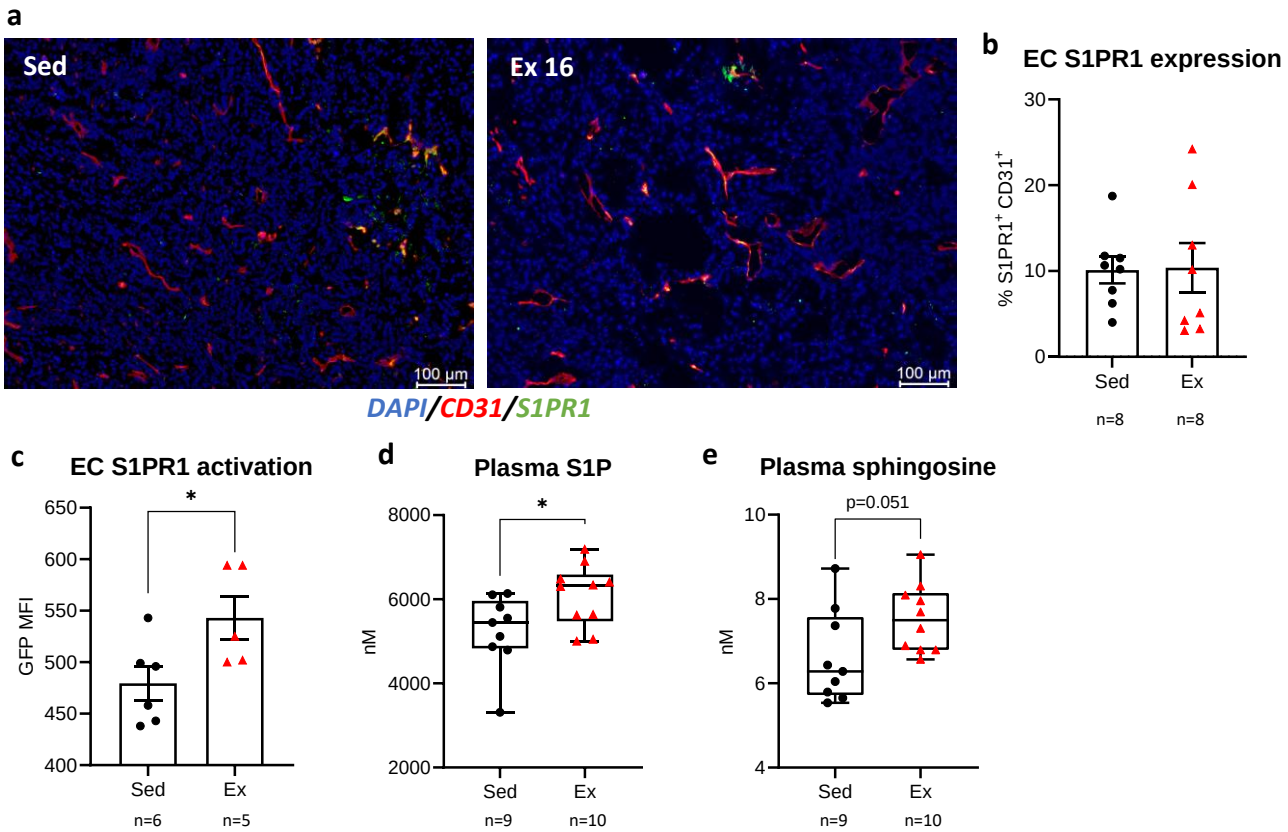
a
Sed
Ex 16
100 µm
100 µm
DAPI/CD31/S1PR1
b
EC S1PR1 expression
% S1PR1+ CD31+
30
20
10
0
Sed
Ex
n=8
n=8
c
EC S1PR1 activation
GFP MFI
650
600
550
500
450
400
*
Sed
Ex
n=6
n=5
d
Plasma S1P
nM
8000
6000
4000
2000
*
Sed
Ex
n=9
n=10
e
Plasma sphingosine
nM
10
8
6
4
p=0.051
Sed
Ex
n=9
n=10

Figure 5

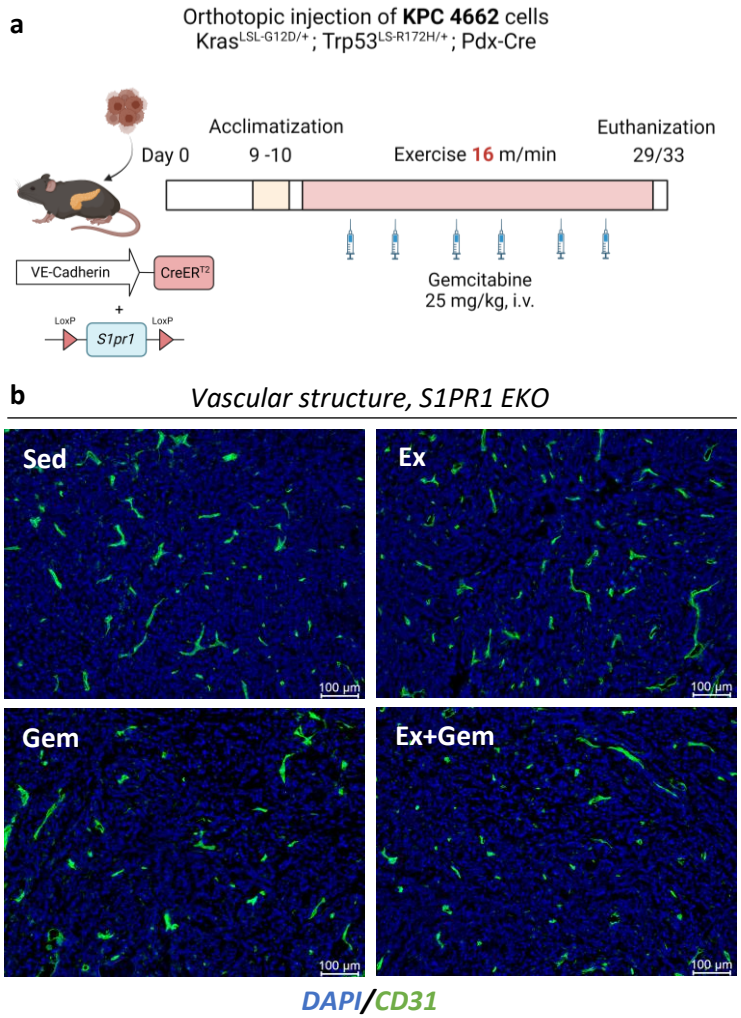
a
Orthotopic injection of KPC 4662 cells
KrasLSL-G12D/+; Trp53LS-R172H/+; Pdx-Cre
Acclimatization
Day 0
9 -10
Exercise 16 m/min
Euthanization
29/33
VE-Cadherin
CreERT2
+
LoxP
S1pr1
LoxP
Gemcitabine
25 mg/kg, i.v.
b
Vascular structure, S1PR1 EKO
Sed
Ex
Gem
Ex+Gem
100 µm
DAPI/CD31

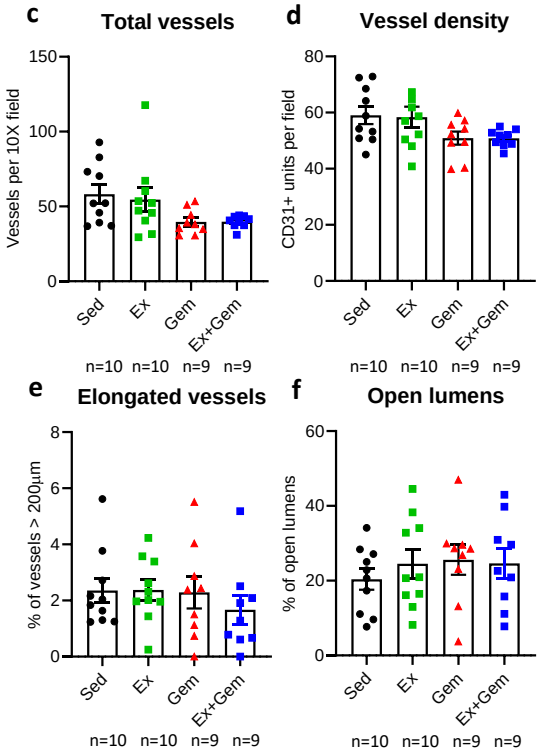
c
Total vessels
Vessels per 10X field
150
100
50
0
Sed
Ex
Gem
Ex+Gem
n=10 n=10 n=9 n=9
d
Vessel density
CD31+ units per field
80
60
40
20
0
Sed
Ex
Gem
Ex+Gem
n=10 n=10 n=9 n=9
e
Elongated vessels
% of vessels > 200µm
8
6
4
2
0
Sed
Ex
Gem
Ex+Gem
n=10 n=10 n=9 n=9
f
Open lumens
% of open lumens
60
40
20
0
Sed
Ex
Gem
Ex+Gem
n=10 n=10 n=9 n=9

Figure 6

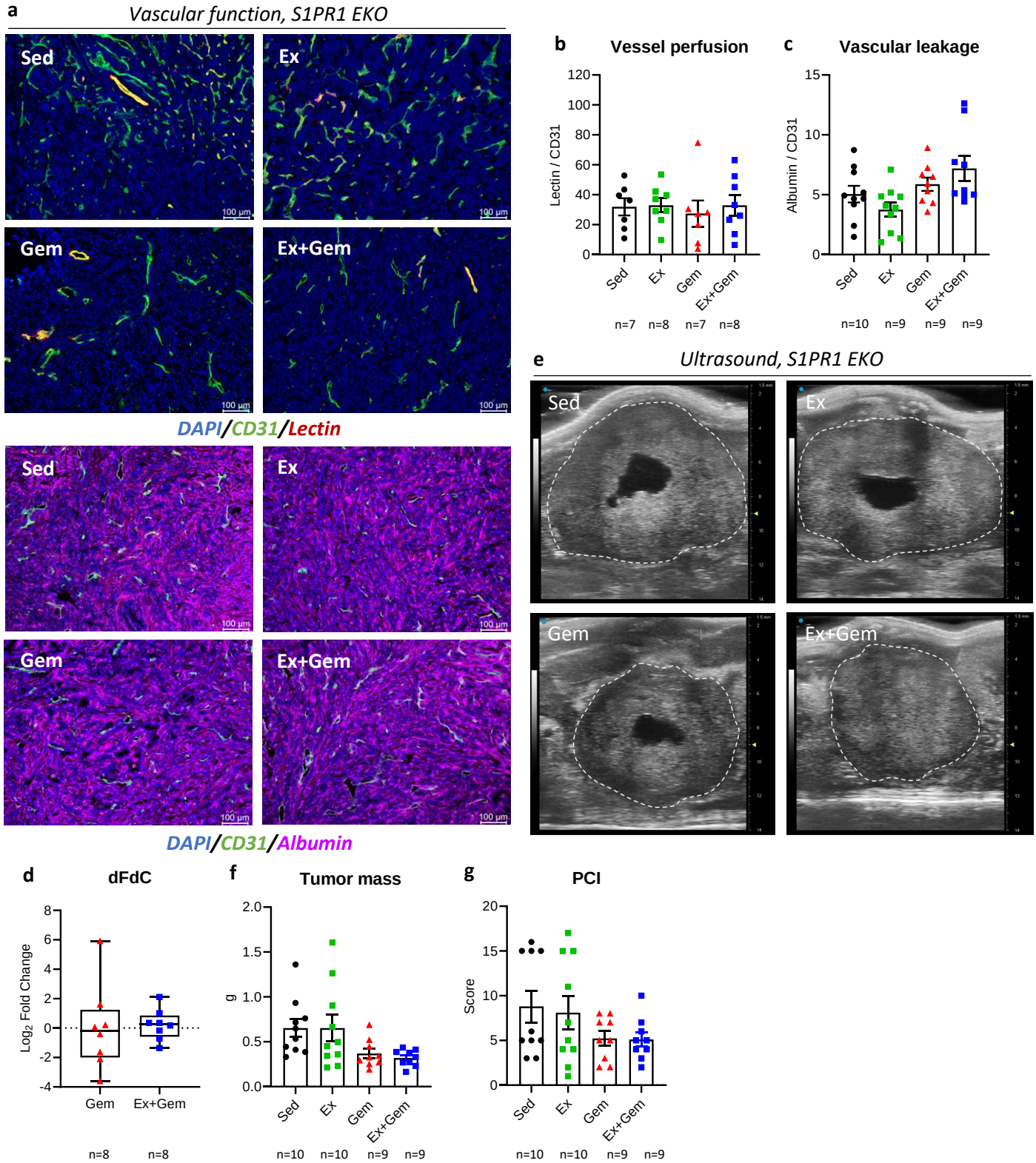
a
Vascular function, S1PR1 EKO
Sed
Ex
Gem
Ex+Gem
100 µm
DAPI/CD31/Lectin
DAPI/CD31/Albumin
b
Vessel perfusion
Lectin / CD31
Sed
Ex
Gem
Ex+Gem
n=7 n=8 n=7 n=8
c
Vascular leakage
Albumin / CD31
n=10 n=9 n=9 n=9
e
Ultrasound, S1PR1 EKO
d
dFdC
Log2 Fold Change
Gem
Ex+Gem
n=8 n=8
f
Tumor mass
g
n=10 n=10 n=9 n=9
g
PCI
Score
n=10 n=10 n=9 n=9

Figure 7

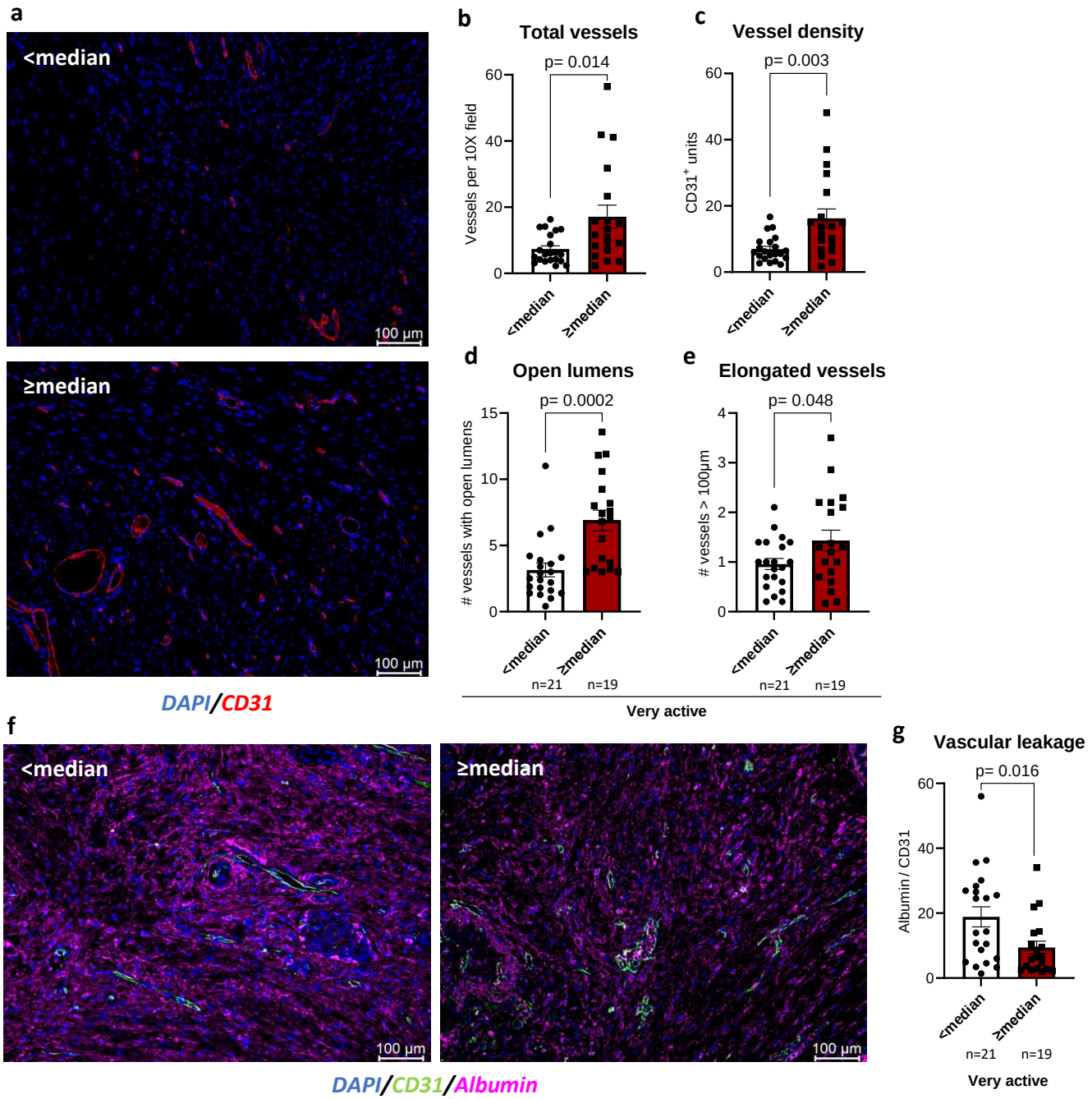
a
<median
100 µm
≥median
100 µm
DAPI/CD31
b
Total vessels
p= 0.014
Vessels per 10X field
60
40
20
0
<median
≥median
c
Vessel density
p= 0.003
CD31+ units
60
40
20
0
<median
≥median
d
Open lumens
p= 0.0002
# vessels with open lumens
15
10
5
0
<median
≥median
n=21
n=19
e
Elongated vessels
p= 0.048
# vessels > 100µm
4
3
2
1
0
<median
≥median
n=21
n=19
Very active
f
<median
100 µm
≥median
100 µm
DAPI/CD31/Albumin
g
Vascular leakage
p= 0.016
Albumin / CD31
60
40
20
0
<median
≥median
n=21
n=19
Very active